

Article

A Study of the Metallurgical and Mechanical Properties of Friction-Stir-Welded Pure Titanium

Michael Regev ^{1,*} , Benny Almozino ¹ and Stefano Spigarelli ² ¹ Department of Mechanical Engineering, Braude College, P.O. Box 78, Karmiel 2161002, Israel² Dipartimento di Ingegneria Industriale e Scienze Matematiche (DIISM), Università Politecnica delle Marche, 60131 Ancona, Italy

* Correspondence: michaelr@braude.ac.il

Abstract: Commercially pure titanium (CP-Ti) plates were friction-stir welded (FSWed) using a welding tool with a tungsten carbide (WC) pin. The bead-on-plate technique was applied to reduce the effects of welding defects, such as incomplete penetration. An X-ray inspection and fractography showed that the FSWed material was free of defects and of WC particles, which may have originated from the welding tool. The appearance of refined equiaxed grains in the thermo-mechanically affected zone (TMAZ) may have been related to dynamic recrystallization (DRX) occurring during the FSW due to the high temperature and intensive plastic deformation involved in the process. Grain refinement, mechanical twinning, and increased dislocation density were detected within the TMAZ, and these microstructural changes were considered to be responsible for the improved mechanical properties of the TMAZ. The TEM study reported in the current paper revealed the presence of nano-sized grains in the FSWed material due to dynamic recrystallization (DRX) occurring during the processing stage. The microstructure obtained during FSW of Ti has been reported in a several publications, yet many discrepancies can be found in these publications. Among these discrepancies are the size and the shape of the grains at the various zones, as well as the presence or non-presence of various zones at the vicinity of the weld. The current study contradicts the argument for correlations between the conditions prevailing at different points across the TMAZ and microstructural changes, which were previously proposed by several researchers.

Keywords: friction-stir welding; CP-Ti; microstructure; mechanical properties; dislocations

Citation: Regev, M.; Almozino, B.; Spigarelli, S. A Study of the Metallurgical and Mechanical Properties of Friction-Stir-Welded Pure Titanium. *Metals* **2023**, *13*, 524. <https://doi.org/10.3390/met13030524>

Academic Editor: João Pedro Oliveira

Received: 7 February 2023

Revised: 2 March 2023

Accepted: 3 March 2023

Published: 5 March 2023



Copyright: © 2023 by the authors. Licensee MDPI, Basel, Switzerland. This article is an open access article distributed under the terms and conditions of the Creative Commons Attribution (CC BY) license (<https://creativecommons.org/licenses/by/4.0/>).

1. Introduction

Titanium and its alloys are known for their high specific strength, high heat resistance, high erosion, and corrosion resistance [1–11]. Hence, they are widely used in aerospace, naval, and military applications, as well as in the chemical, biomedical, and nuclear industries [1–11].

The application of fusion welding may result in grain coarsening, a high level of porosity, and the formation of undesirable brittle coarse cast structures and Ti oxide, in addition to residual stresses and distortion [1–7]. Friction-stir welding (FSW) has the potential to overcome these disadvantages and serve as an alternative method to the more conventional fusion-welding techniques. Friction-stir welding is a solid connection method invented by the Welding Institute, UK, in 1991 [5]. The key advantage of FSW over conventional fusion-welding techniques is that it achieves a metallic bond below the melting point of the base material, thus avoiding many of the metallurgical problems associated with the solidification process.

Friction-stir welding has been successfully applied to various Al, Mg, and Cu alloys, as well as cast iron, carbon steel, and stainless steels [1,2,4]. However, applying FSW to Ti using conventional welding tools made of tool steel is difficult due to Ti's high melting temperature (1668 °C). The complexity arising from the relatively high melting point of Ti

has been the topic of several publications dealing with FSW of Ti and its alloys, yet only a few of these articles refer to pure Ti [1–9,12–15]. More temperature-wear-resistant materials are required for the FSW of CP-Ti. These materials include polycrystalline cubic boron nitride (pcBN) [1], TiC [2], bi-material tools with WC pins and W shoulders [3], WC [7,12], W [8], W-25at.% Re [9], Mo-based alloy [12,13], WC-Co [14], and W-La [15].

Several publications dealt with the microstructure obtained during the FSW of Ti [1–9,12–15]. However, many discrepancies can be found in these publications, including the sizes and shapes of the grains in the various zones. Zhang et al. [1] reported fine grain refinement of equiaxed grains from 27 μm in the parent metal (PM) down to 13 μm , with serrated boundaries, in all the regions of the stir zone (SZ), with the slight occurrence of twin boundaries. Lee et al. [2] reported grain coarsening in the nugget with a large amount of twinning. Jiang et al. [11] reported grain refinement of about an order of magnitude at the stir zone. Fujii et al. [4] and Kang and Lee [12] reported various degrees of grain refinement at the SZ as a function of the welding parameters. According to Mironov et al. [13], the SZ is composed of fine equiaxed grains with no heat-affected zone (HAZ) detected. These authors showed that the TMAZ can be divided into three sub-regions based on the size and aspect ratio of the grains, without any discernible differences between the advancing side and the retreating side. Liu et al. [14] studied the FSW of lap joints and found that the deformation direction could be identified in the TMAZ, while the SZ underwent grain refinement from an average parent-metal grain size of 22 μm down to 4–8 μm . Bahl et al. [8] reported grain refinement at the SZ from 57 μm down to 19 μm . They also found that the grains of the SZ had serrated boundaries rather than being perfectly equiaxed. Xu et al. [7] studied the influence of the cooling conditions and reported both grain refinement and twinning in the SZ.

Another example of discrepancies regarding the FSW of Ti relates to the presence of various zones at the vicinity of the weld. Zhang et al. [1] reported the absence of any thermo-mechanically affected zones (TMAZ), whereas Lee et al. [2] reported the presence of a TMAZ and of a softened HAZ next to the TMAZ. Seighalani et al. [3] claimed that no TMAZ was detected, yet they pointed to the presence of a HAZ. Mironov et al. [13] and Liu et al. [14] reported the presence of a SZ and a TMAZ, whereas Bahl et al. [8] reported that the TMAZ and HAZ were difficult to detect.

In light of these discrepancies and others, and in the absence of microstructural mapping of the various zones at different depths, the authors of this paper concluded that an independent comprehensive microstructure study is necessary as a preliminary stage. The current paper focuses on the mechanical properties, namely tension and hardness, as well as on fractography and a quantitative transmission electron microscopy (TEM) study comparing the parent material and the stir zone of FSWed CP-Ti. The authors decided to use bead-on-plate specimens rather than “real” butt-welded specimens in order to rule out the influence of certain FSW defects, such as incomplete penetration, on the mechanical properties, thereby guaranteeing that the mechanical properties would be dictated solely by the microstructural changes. It should be noted that none of the publications mentioned above reported a study based on the bead-on-plate technique. Almost all of the studies dealt with butt welding on 2-millimeter-thick plates [4,7], 3-millimeter-thick plates [1,3,13], 5.6-millimeter-thick plates [2], or 6.35-millimeter-thick plates [13], while one publication [14] dealt with the FSW of lap joints. In addition to examining the influence of the welding process on the mechanical properties and the microstructure, the current paper proposes ways to settle some of the aforementioned discrepancies.

2. Materials and Methods

2.1. FSW-Process Optimization

The material used for this study was commercially pure grade 2 Ti in the form of plates measuring 200 mm \times 200 mm, 3 mm thick. These plates were subjected to bead-on-plate FSW using a M32 CNC milling machine (Sharno Computerized Machines Ltd., Petach

Tikva, Israel). The welding tool was made of H-13 tool steel with a 20-millimeter-diameter shoulder and a 2-millimeter-long WC pin, as shown in Figure 1.

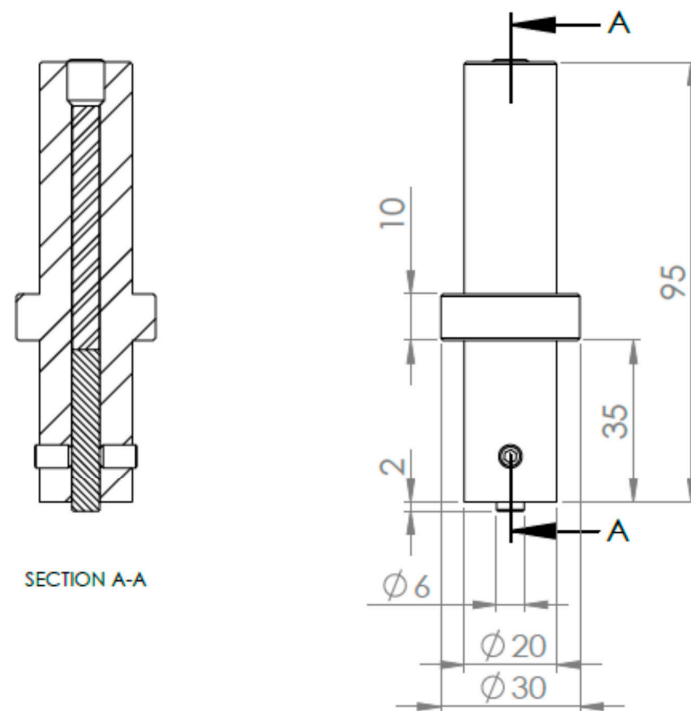


Figure 1. The welding tool.

Welding optimization was achieved by using different experimental conditions, as listed in Table 1. To heat up the plate before welding started, the pin was rotated in its place for one minute after penetration and at the point when the shoulder was brought into contact with the upper surface of the plate. As a result, the welding tool turned bright red, indicating that it had reached a temperature higher than 750 °C. The criteria for selecting the optimal welding parameters included the integrity of the pin after two consecutive passes, each 80 mm long, together with visual examination of the weld. According to these criteria, the preferred welding parameters were found to be a rotational speed of 700 rpm and a transverse speed of 50 mm/min. After approximately 160 mm of welding, the shoulder of the welding tool developed a mushroom shape. Each welding tool was replaced after 80 mm of welding in order to avoid the influence of shoulder deformation. Four metallographic specimens were then extracted from a plate welded under these parameters. The first metallographic specimen was taken from the first quarter of the seam, the second from the second quarter, and so on, in order to rule out the presence of inner porosity or cracking. All the welded specimens were then radiographically checked. Analysis of the X-ray-inspection results showed that a rotational speed of $\omega = 700$ rpm and a transverse speed of $v = 50$ mm/min yielded a defect-free stir zone. These were therefore chosen as the welding parameters.

Table 1. FSW list of experiments.

Experiment	ω (rpm)	v (mm/min)
1	700	35
2	700	35
3	1250	35
4	1100	500

Table 1. *Cont.*

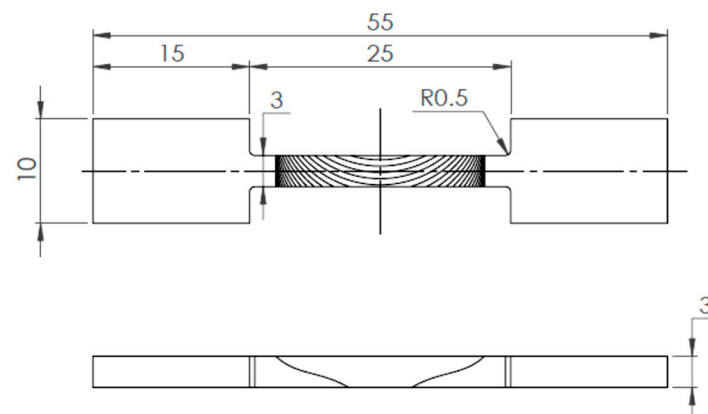
Experiment	ω (rpm)	v (mm/min)
5	250	25
6	700	35
7	700	25
8	700	25
9	500	50

2.2. Metallography

The metallographic study was conducted using a Zeiss AX10 optical microscope and a Quanta 200 environmental-scanning electron microscope (E-SEM) equipped with an energy dispersive X-ray spectroscopy (EDS) system (FEI Technologies Inc., Hillsboro, OR, USA).

2.3. Mechanical Properties

Vickers microhardness measurements were taken using a microhardness tester (Shimadzu, Corporation, Kyoto, Japan) under a load of 200 gf. Tensile specimens with a square cross-section measuring 3 mm \times 3 mm and a gauge length of 25 mm were machined from the FSW region of the plates. The longitudinal axis of the samples was perpendicular to the FSW direction, as shown in Figure 2. Five tensile tests were carried out on the PM, while six tensile tests were carried out on FSWed material.

**Figure 2.** Drawing of a tensile specimen.

2.4. TEM

The TEM investigation was conducted using a Tecnai G2 T20 TEM. The TEM specimens were prepared using an FEI Helios NanoLab G3 focused ion beam (FIB) (FEI Technologies Inc., Hillsboro, OR, USA).

2.5. Fractography

The fractography study was conducted on broken friction-stir-welded creep specimens with the aid of an Inspect SEM (FEI Technologies Inc., Hillsboro, OR, USA).

3. Results

Figure 3 shows an optical micrograph of the parent metal. The figure indicates that the grains of the parent metal were equiaxed, with an average size of about 20–30 μm .

Optical micrographs of the weld are shown in Figure 4. Figure 4a shows the cross-section under low magnification, with the various points at which the optical micrographs shown in Figure 4b–j were taken. Points 1–3 are located at the center of the stir zone at

depths of 0.6, 1.6, and 2.4 mm from its upper surface, respectively. Points 4–6 are located at the same depths next to the interface, with the parent metal on the advancing side (AS), and points 7–9 are located at the same depths next to the interface, with the parent metal on the retreating side (RS).

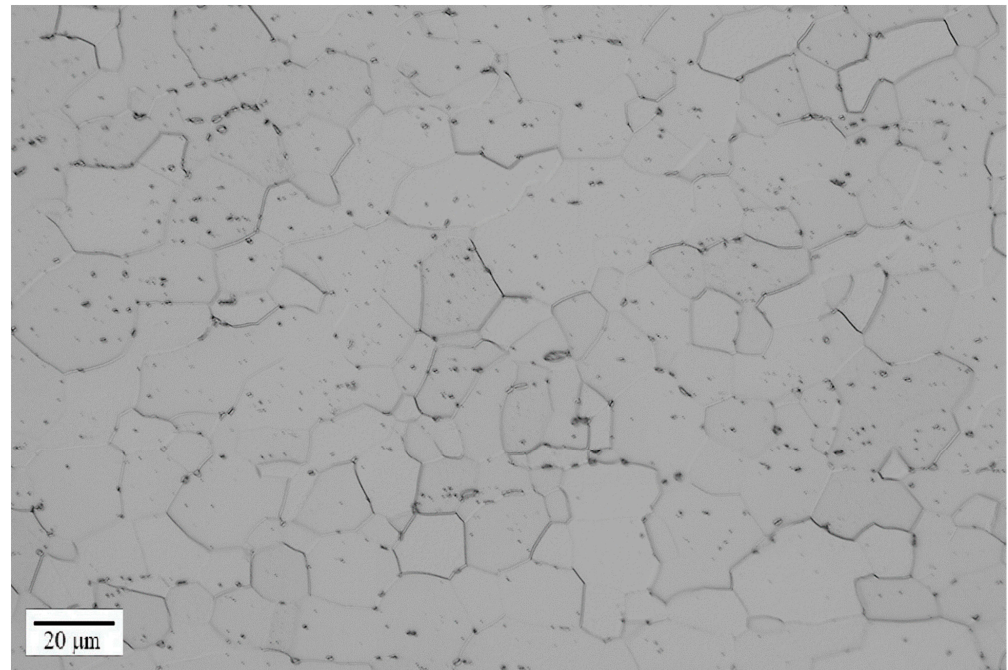


Figure 3. Optical micrograph of the parent metal.

Figure 4b,c show that the microstructure of the upper part of the SZ (points 1 and 2)—namely, at depths of 0.6 mm and 1.6 mm—contained twins, whereas point 3 (Figure 4d) was characterized by equiaxed fine grains with an average size of 2–3 μm. Figure 4e–g show that the microstructure of the RS of the TMAZ changed from a twin microstructure at the upper part (Figure 4e) to a refined microstructure with boundaries that were serrated to some extent (Figure 4f,g). The grain size in both cases varied from submicron sizes to 1–2 microns, in turn indicating that the microstructure was finer than that observed at the bottom of the stir zone (Figure 4d). Regarding the AS, serrated grain boundaries can be seen in the upper part (Figure 4h), whereas in the case of point 8 (Figure 4i), a coarse twin structure can be seen, similar to that of points 1 and 2. An equiaxed microstructure can be observed in the case of point 9 (Figure 4j), with a grain size similar to that of point 3. Note that the aforementioned equiaxed grains were one order of magnitude finer than the grains of the parent material. The EDS analysis conducted next to the upper surface of the weld at ten different points across the weld ruled out the presence of any WC particles separated from the pin. Table 2 summarizes the main characteristics of the microstructures observed at points 1–9 in Figure 4a.

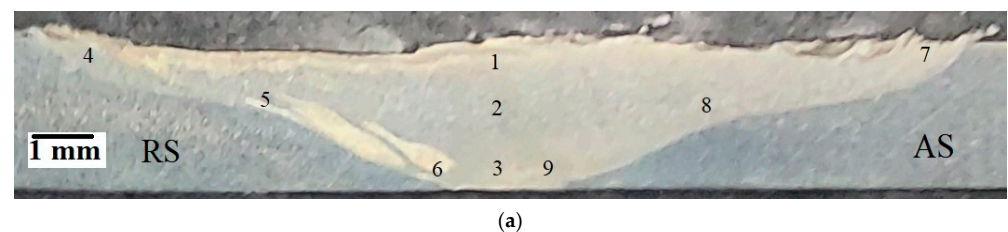


Figure 4. Cont.

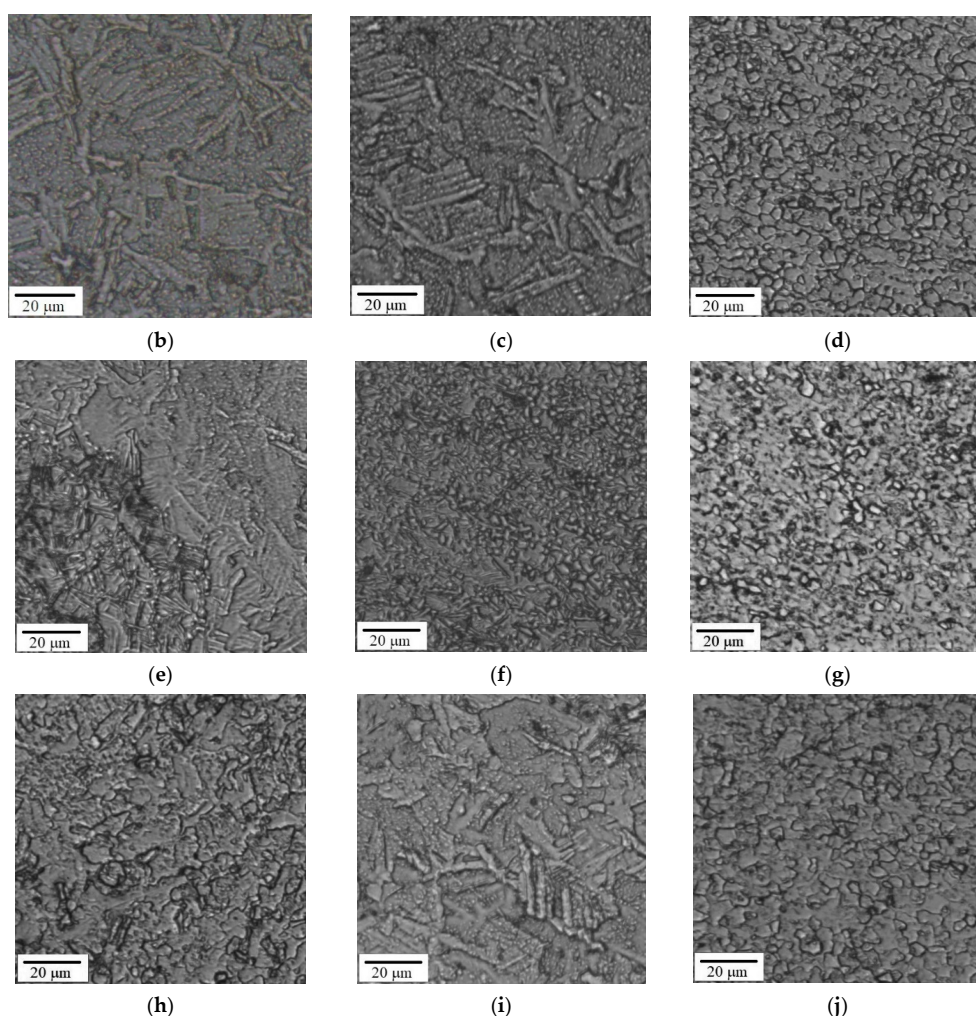


Figure 4. Optical micrographs of the weld: (a) cross-section showing the points from which micrographs (b–j) were taken; (b) optical micrograph taken at point 1; (c) optical micrograph taken at point 2; (d) optical micrograph taken at point 3; (e) optical micrograph taken at point 4; (f) optical micrograph taken at point 5; (g) optical micrograph taken at point 6; (h) optical micrograph taken at point 7; (i) optical micrograph taken at point 8; (j) optical micrograph taken at point 9.

Table 2. Microstructure characteristics.

Point	Microstructure
1	Twin structure
2	Twin structure
3	Equiaxed grains with an average size of 2–3 μm
4	Twin microstructure
5	Refined microstructure, grain size varies from submicron size to 1–2 microns, the grain boundaries are serrated to some extent
6	Refined microstructure, grain size varies from submicron size to 1–2 microns, the grain boundaries are serrated to some extent
7	Serrated grain boundaries
8	Twin structure
9	Equiaxed grains with an average size of 2–3 μm

Figure 5 depicts an optical micrograph of the interface between the weld and the PM at the RS. It was taken near point 5 in Figure 4a. The figure shows that the PM grain size was similar to that in Figure 3.

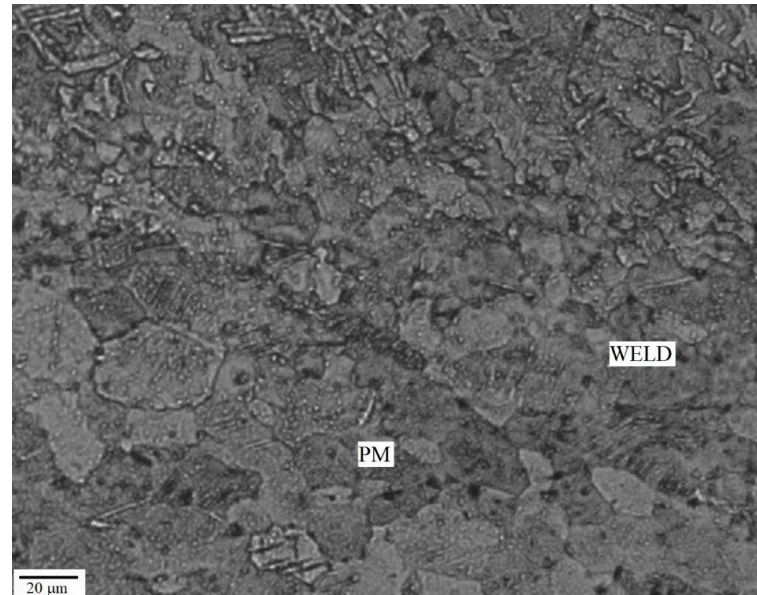


Figure 5. The interface between the PM and the weld.

Figure 6a–c depict three microhardness profiles taken across the weld at depths of 0.6, 1.6, and 2.4 from its upper surface, respectively. All the measurements were taken across the stir zone and the adjacent zones, perpendicular to the longitudinal axis of the weld, while maintaining a distance of 0.5 mm from one indentation to another. The measurement began and ended at the parent metal.

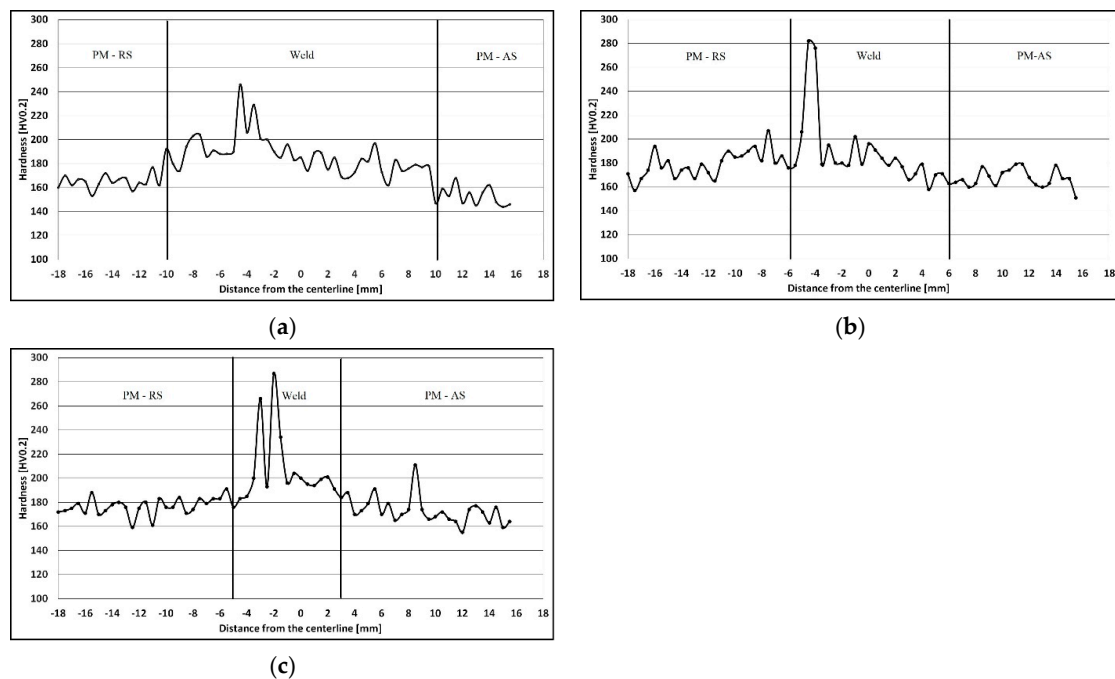


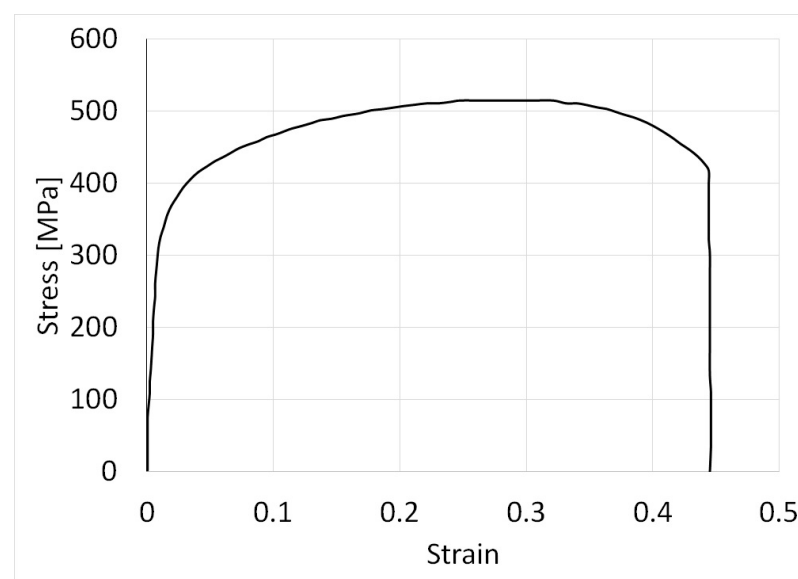
Figure 6. Microhardness profiles taken across the weld at various depths: (a) 0.8 mm; (b) 1.6 mm; (c) 2.4 mm.

The vertical lines shown in Figure 6a–c represent the border between the weld and the PM at the respective depths. The different optical contrasts under low magnification revealed the location of the boundary lines at given depths (Figure 4a). The observation at the weld zone showed that the hardness was slightly higher at the RS than at the AS. The highest hardness values—namely, 246 and 229 HV0.2 in the case of Figure 6a, 282 and 276 in the case of Figure 6b, and 266 and 287 in the case of Figure 6c—were taken from the bright bands seen between points 5 and 6 in Figure 4a.

Figure 7a depicts a typical stress–strain curve of a PM specimen, while Figure 7b refers to a FSWed specimen. Table 3 summarizes the tensile-test results for the parent material, as well as for the FSWed specimens. As can be seen in Table 3, both the yield strength and the ultimate tensile strength (UTS) of the FSWed material were not inferior to those of the parent material, while the elongation of the FSWed material was markedly lower. All the FSWed specimens failed at the PM of the AS.

Figure 8a provides a general view of the fracture surface of a broken parent-material tensile specimen, and Figure 8b shows the fracture surface of a broken FSWed specimen. Both micrographs were taken at the central part of the fracture surface using an SEM under the same magnification. It is evident that both fracture surfaces had a ductile fracture character. In the case of the PM, the voids tended to be more uniformly sized, as indicated by the arrows. The FSWed specimen, however, showed some variations. The arrows in Figure 8b point to two neighboring voids that differ in size by an order of magnitude. The surfaces of all the fracture specimens were observed, and none of them showed evidence of pre-existing cracks or other defects.

Figure 9a is a bright field (BF) TEM micrograph of the parent material taken near the $\langle 5143 \rangle$ zone axis (Z.A.) showing randomly distributed dislocations, as indicated by arrows. Figure 9b shows the selected area electron diffraction pattern (SADP) of the relevant selected area. Figure 9c shows BF TEM micrographs taken from the TMAZ of the FSWed material (for the exact definition of the TMAZ used in this paper, see first paragraph of the discussion). The dark grain in Figure 9c (grain 1) was tilted to $\langle \bar{1}2\bar{1}6 \rangle$ Z.A. Figure 9d shows its SADP, and Figure 9e,f show the SADPs of two neighboring grains. Figure 9e,f correspond to grains 2 and 3 in Figure 9c. The different SADPs, together with the dark contrast typical of grains tilted to a certain zone axis, indicate that these were separate grains rather than sub-grains. The average size of the grains discernible in Figure 9c was about 50 nm, and no dislocations were detected inside the grains. The fineness of these grains made it difficult to obtain a single-grain SADP.



(a)

Figure 7. Cont.

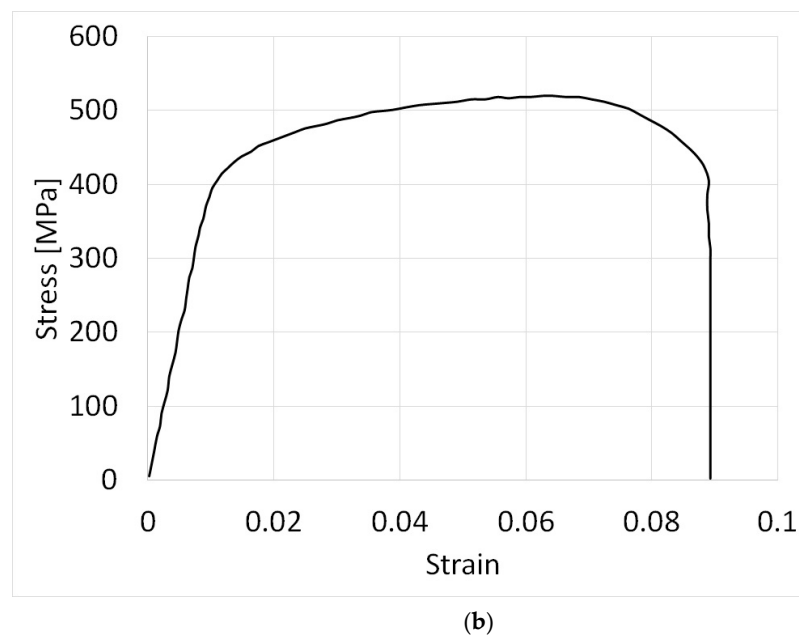


Figure 7. Stress–strain curves of: (a) parent-metal specimen; (b) friction-stir-welded specimen.

Table 3. Tensile-test results.

Type	Average Yield Strength (MPa)	Yield Strength S.D. (MPa)	Average UTS (MPa)	UTS S.D. (MPa)	Average Elongation (%)	Elongation S.D. (%)
PM	325.4	27.4	504.6	10.8	37.6	4.8
FSW'ed	400.8	37.1	507.8	33.6	8.5	2.3

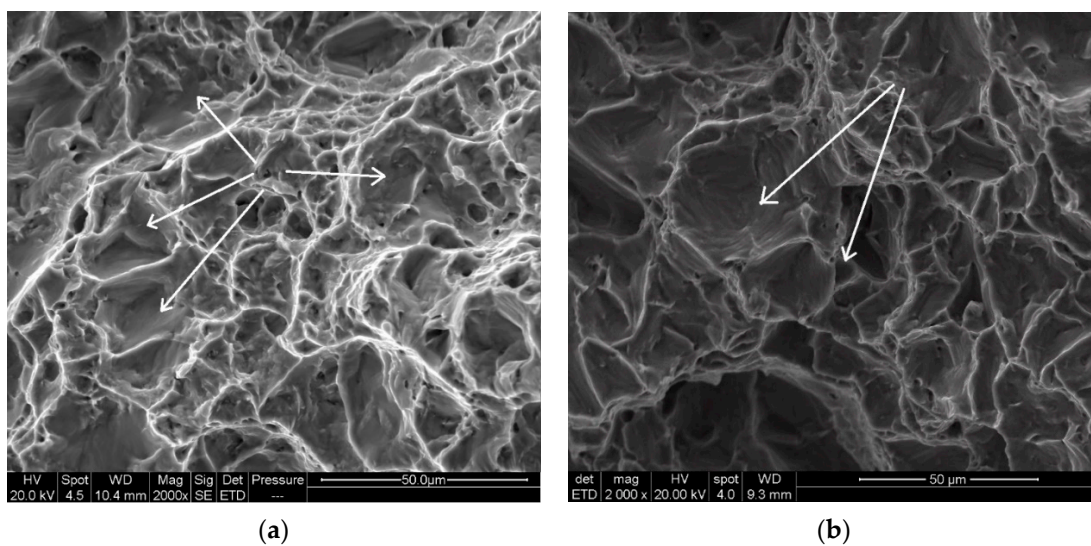


Figure 8. SEM micrographs of the fracture surface of broken tensile specimens: (a) parent material; (b) FSWed specimen.

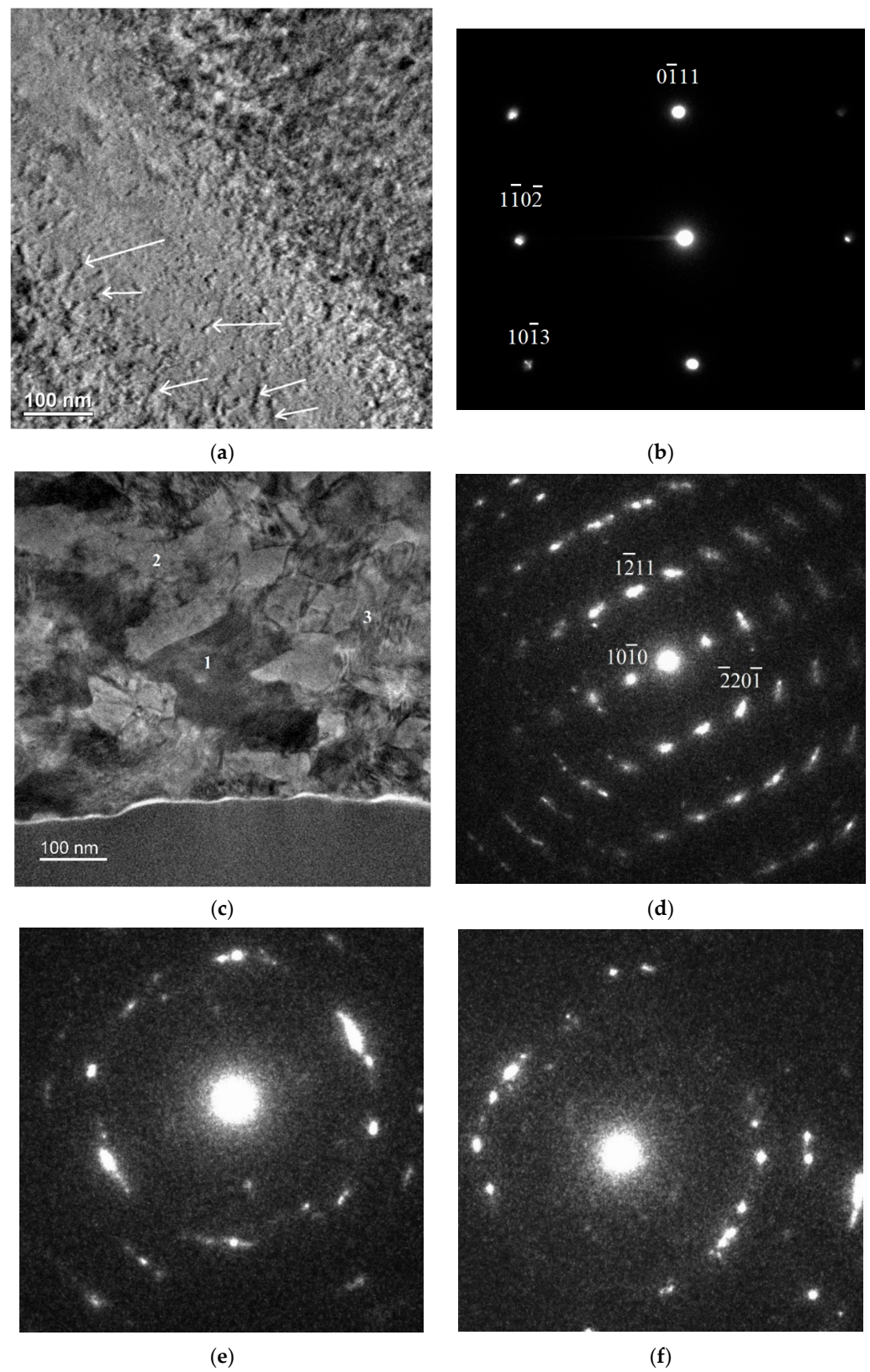


Figure 9. (a) TEM BF micrograph of the FSWed material taken near $\langle 5\bar{1}43 \rangle$ Z.A.; (b) SADP of $\langle 5\bar{1}43 \rangle$ Z.A.; (c) BF image of the FSWed material taken near $\langle \bar{1}2\bar{1}6 \rangle$ Z.A.; (d) SADP of $\langle \bar{1}2\bar{1}6 \rangle$ Z.A.; (e) SADP of grain 2; (f) SADP of grain 3.

4. Discussion

As stated above, reports in the literature regarding the presence or absence of various zones in the vicinity of the weld are ambiguous. According to Mishra and Mahoney [16], the history of the FSW nomenclature was as follows. Early in the development of FSW, the term TMAZ referred to the region between the SZ and the HAZ. This region underwent both temperature and plastic deformation, yet the deformation was insufficient for full recrystallization, as occurs at the SZ. This nomenclature was convenient for Al alloys, in which these three distinct zones can be clearly identified. However, this definition of the TMAZ was found to be inappropriate for cases in which a distinct TMAZ was not evident. It was decided, therefore, to redefine the TMAZ to include all the regions affected by heat and deformation with the SZ subset within the TMAZ. Nevertheless, the original definitions continue to be used. This explanation may resolve the discrepancies mentioned above regarding the presence of the various zones. As can be seen in Figure 4, it is impossible to distinguish between the SZ and the TMAZ. Hence, the authors of this paper find the new definition more appropriate for the current case and therefore use it in this discussion.

The location of points 1–3 in Figure 4 leads to the assumption that Figure 4a–c were taken from the SZ, although, as stated above, its borders were not clear. Lee et al. [2] attributed the appearance of a dense twin structure in the upper-middle part of the TMAZ to a more severe plastic deformation due to direct contact with the shoulder of the welding tool. Note that Lee et al. studied this zone, which they believed was the SZ, at one single location near its middle. In contrast, they studied the upper part next to the point where the TMAZ bordered on its AS, so they did not distinguish between the SZ and the rest of the TMAZ. Contrary to Lee et al., Zhang et al. [1] studied the microstructure of the SZ at three different depths, similar to the current study. They reported serrated grain boundaries without twins throughout the SZ and attributed the appearance of these serrated grain boundaries to the allotropic transformation of the α phase occurring when the peak temperature exceeded 885 °C. However, Zhang et al. did not study the microstructure of the TMAZ at various depths, as in the current study. Indeed, the current study revealed a twin structure in the middle and the upper parts of the SZ, in line with Lee et al. [2]. Regarding the TMAZ, in the current study, the microstructure was found to change from a twin structure to refined grains, with boundaries serrated to some extent at the RS, followed by a shift from grains with serrated boundaries to twin structures, and then to equiaxed boundaries in the AS. The appearance of the twins may have been related to the severe plastic deformation, whereas the appearance of equiaxed grains at the bottom of the SZ and the TMAZ that were an order of magnitude finer than the grains of the PM (see Figure 3) may have been related to dynamic recrystallization (DRX). Bahl et al. [8] analyzed the DRX mechanisms operating during the FSW of Ti and reached the conclusion that all three DRX mechanisms—namely, discontinuous dynamic recrystallization (DDRX), geometric dynamic recrystallization (GDRX), and continuous dynamic recrystallization (CDRX)—were operative. Xu et al. [7] claimed that twinning is expected at lower temperatures than in DRX. Nevertheless, the current study examined the occurrence of both processes at given depths, and, hence, at given temperatures, such as points 5, 2, and 8 (Figure 4c,f,i, respectively), and the results obtained do not support this claim. Furthermore, points 1 (Figure 4b) and 3 (Figure 4i) had twin structures and were the points closest to and farthest away from the shoulder, meaning that they were the hottest and coolest points, respectively, whereas point 2 (Figure 4f) had an equiaxed structure in the middle of the cross-section. It is possible to conclude that the DRX occurring during FSW was responsible for the formation of these grains.

Neither grain coarsening nor softening were recorded in the zone adjacent to the TMAZ, as can be seen in Figures 5 and 6, leading to the conclusion that no HAZ could be identified. Some of the researchers mentioned above noted the absence of an HAZ. The increased hardness of the TMAZ may be related both to the mechanical twinning and to the grain refinement observed in this zone. The occurrence of the fracture at the AS during the tension test was in line with the results reported by Reshad Seighalani et al. [3], but

in contrast to those of Lee et al. [2], who reported that the fracture always occurred at the RS. Figure 6 indicates that the PM at the AS was, to some extent, softer than that of the RS, possibly explaining the location of the fracture. According to Table 3, the average elongation to fracture for the FSWed material was about 23% of the PM. Since the AS was the site not only of the fracture, but also most of the plastic deformation, particularly the necking, one should refer to the length of the AS segment of the tensile specimen as if it were the specimen's initial length or close to it. According to Figure 4a, the SZ length changed from 20 mm at the upper surface to 3 mm at the lower surface. Accordingly, the AS segment was about 6.75 mm long, on average. This length was about 27% of the initial length of the PM specimens and was, therefore, in line with the different values of the elongations to fracture. As stated above, both fracture surfaces had a ductile fracture character (Figure 7a,b, which was expected, since all the FSWed specimens failed at the PM of the AS. Differences in void-size distribution do not appear to affect mechanical properties.

Further evidence of DRX was provided by the TEM study. In Figure 9a, the entire region taken from the PM was part of one grain, as shown by the SADP of this grain (Figure 9b). Contrary to the PM, a TEM study of the processed material yielded very low dislocation density, as can be seen in Figure 9c. It seems that the microstructure consisted of ultrafine grains. In support of this claim, the TEM specimen was tilted to arbitrary zone axes of certain grains. This action was based on the fact that when a crystal is tilted to a certain zone axis, such as $\langle \bar{1}2\bar{1}6 \rangle$ in Figure 9d, its BF image becomes darker (see grain 1 in Figure 9c), since more energy passes from the incident beam to the diffracted beams. This phenomenon can be used to distinguish between two adjacent grains, as well as to measure grain size. Based on the repetition of this procedure on a sufficiently large number of grains, it seems that both the absence of dislocations and the results of these tilting experiments show that the FSWed material was composed mostly of ultrafine grains created during FSP. The presence of such an ultrafine dislocation free grains may have been related to the DRX. Finally, it seems clear that the severe plastic deformation and the high temperatures prevailing during FSW are responsible both for mechanical twinning and for DRX, which in turn leads to grain refinement

In summary, although microstructural changes occurred during the FSW due to severe plastic deformation and exposure to high temperatures, the mechanical properties of the FSWed specimens were not inferior to those of the PM. The TMAZ was found to be harder than the adjacent PM. The average values of the UTS of the PM and of the FSWed material were approximately similar, and the average values of the yield strength of the FSWed material were found to be more than 20% higher than those of the PM. The strengthening mechanisms operating in the TMAZ were those reported in previous works, namely, grain refinement due to DRX and mechanical twinning. Nevertheless, neither of the two previous attempts to establish connections between these processes and the location of their respective microstructures based on temperature changes seem to fit the current results. The technological implication of the current study is that the welding process is safe as far as the mechanical properties at room temperature are concerned.

5. Conclusions

The CP-Ti underwent bead-on-plate FSW with the aid of an H13 tool with a WC pin, yielding a defect-free weld.

The X-ray inspection and EDS analysis ruled out the presence of WC particles and other sources of contamination inside the stir zone.

The presence of refined equiaxed grains in the TMAZ was related to the DRX.

Grain refinement and mechanical twinning were detected inside the TMAZ and the stir zone by means of optical microscopy, SEM, and TEM.

The fractography study results showed that the fracture had the same ductile character, and no pre-existing cracks or other defects were observed in either the parent or the FSWed material.

The mechanical properties of the FSWed material at room temperature were superior to those of the parent material.

A further quantitative analysis is still required to correlate between the microstructure and the conditions prevailing across the TMAZ

Author Contributions: Conceptualization, M.R. and S.S.; methodology, M.R. and S.S.; validation, M.R. and S.S.; formal analysis, M.R., S.S.; investigation, M.R., B.A., and S.S.; data curation, M.R. and B.A.; writing—original draft, M.R.; writing—review and editing, M.R.; visualization, M.R.; funding acquisition, M.R.; All authors have read and agreed to the published version of the manuscript.

Funding: This research project is partially funded by Braude College, Karmiel, Israel.

Data Availability Statement: The data presented in this study are available on request from the corresponding author.

Acknowledgments: The assistance of N. Navot with welding the material is highly appreciated. The authors thank E. Kesselman for her assistance with the TEM study and Y. Zilberman for TEM specimen preparation. Thanks are also due to A. Katz-Demyanetz for his assistance with the SEM study.

Conflicts of Interest: The authors declare no conflict of interest.

References

1. Zhang, Y.; Sato, Y.S.; Kokawa, H.; Park, S.H.C.; Hirano, S. Stir zone microstructure of commercial purity titanium friction stir welded using pcBN tool. *Mater. Sci. Eng. A* **2008**, *488*, 25–30. [[CrossRef](#)]
2. Lee, W.B.; Lee, C.Y.; Chang, W.S.; Yeon, Y.M.; Jung, S.B. Microstructural investigation of friction stir welded pure titanium. *Mater. Lett.* **2005**, *59*, 3315–3318. [[CrossRef](#)]
3. Reshad Seighalani, K.; Besharati Givi, M.K.; Nasiri, A.M.; Behemat, P. Investigations on the effects of the tool material, geometry, and tilt angle on friction stir welding of pure titanium. *J. Mater. Eng. Perform.* **2010**, *19*, 955–962. [[CrossRef](#)]
4. Fujii, H.; Sun, Y.; Kato, H.; Nakata, K. Investigation of welding parameter dependent microstructure and mechanical properties in friction stir welded pure Ti joints. *Mater. Sci. Eng. A* **2010**, *527*, 3386–3391. [[CrossRef](#)]
5. Kim, J.D.; Jin, E.G.; Murugan, S.P.; Park, Y.D. Recent advances in friction-stir welding process and microstructural investigation of friction stir welded pure titanium. *J. Weld. Join.* **2017**, *35*, 6–15. [[CrossRef](#)]
6. Karna, S.; Cheepu, M.; Venkateswarulu, D.; Srikanth, V. Recent developments and research progress on friction stir welding of titanium alloys: An overview. *IOP Conf. Ser. Mater. Sci. Eng.* **2018**, *330*, 012068. [[CrossRef](#)]
7. Xu, N.; Song, Q.; Bao, Y.; Jiang, Y.; Shen, J.; Cao, X. Twinning-induced mechanical properties' modification of CP-Ti by friction stir welding associated with simultaneous backward cooling. *Sci. Technol. Weld. Join.* **2017**, *7*, 610–616. [[CrossRef](#)]
8. Bahl, S.; Nithilaksh, P.L.; Suwas, S.; Kailas, S.V.; Chatterjee, K. Processing–microstructure–crystallographic texture–surface property relationships in friction stir processing of titanium. *J. Mater. Eng. Perform.* **2017**, *26*, 4206–4216. [[CrossRef](#)]
9. Jiang, L.; Huang, W.; Liu, C.; Chai, L.; Yang, X.; Xu, Q. Microstructure, texture evolution and mechanical properties of pure Ti by friction stir processing with slow rotation speed. *Mater. Charact.* **2019**, *148*, 1–8. [[CrossRef](#)]
10. Callegari, B.; Oliviera, J.P.; Aristizabal, K.; Coelho, R.S.; Brito, P.P.; Wu, L.; Schell, N.; Soldera, F.A.; Mucklich, F.; Pinto, H.C. In-situ synchrotron radiation study of the aging response of Ti-6Al-4V alloy with different starting microstructures. *Mater. Charact.* **2020**, *165*, 110400. [[CrossRef](#)]
11. Callegari, B.; Oliviera, J.P.; Coelho, R.S.; Brito, P.P.; Schell, N.; Soldera, F.A.; Mucklich, F.; Sadik, M.I.; Garcia, J.L.; Pinto, H.C. New insights into the microstructural evolution of Ti-5Al-5Mo-5V-3Cr alloy during hot working. *Mater. Charact.* **2020**, *162*, 110180. [[CrossRef](#)]
12. Kang, D.S.; Lee, K.J. Recent R&D status on friction stir welding of Ti and its alloys. *J. Weld. Join.* **2015**, *33*, 1–7.
13. Mironov, S.; Sato, Y.S.; Kokawa, H. Development of grain structure during friction stir welding of pure titanium. *Acta Mater.* **2009**, *57*, 4519–4528. [[CrossRef](#)]
14. Liu, H.; Nakata, K.; Yamamoto, N.; Liao, J. Friction stir welding of pure titanium lap joint. *Sci. Technol. Weld. Join.* **2010**, *15*, 428–432. [[CrossRef](#)]
15. Fonda, R.W.; Knipling, K.E.; Levinson, A.J.; Feng, C.R. Enhancing the weldability of CP titanium friction stir welds with elemental foils. *Sci. Technol. Weld. Join.* **2019**, *24*, 617–623. [[CrossRef](#)]
16. Mahoney, W.M. Mechanical properties of friction stir welded aluminum alloys. In *Friction Stir Welding and Processing*, 1st ed.; Mishra, R.S., Mahoney, W.M., Eds.; ASM International: Materials Park, OH, USA, 2007; p. 72.

Disclaimer/Publisher's Note: The statements, opinions and data contained in all publications are solely those of the individual author(s) and contributor(s) and not of MDPI and/or the editor(s). MDPI and/or the editor(s) disclaim responsibility for any injury to people or property resulting from any ideas, methods, instructions or products referred to in the content.